Ligand-controlled alteration of nuclear trajectories during photoinduced intersystem crossing in bis-meridional Fe^{II} complexes

Ryan T. Ash,[a] Kaili Zhang, [a] Conor D. Rankine,[b] Justin T. Malme,[a] Thomas J. Penfold,[b] Gregory S. Girolami[a] and Josh Vura-Weis[a*]

[a] Department of Chemistry, University of Illinois at Urbana-Champaign, Urbana, Illinois, 61801, USA.
[b] Chemistry, School of Natural and Environmental Sciences, Newcastle University, Newcastle upon Tyne, UK

Abstract

The intersystem crossing dynamics of two bis-meridional iron(II) complexes are studied by femtosecond transient M-edge X-ray near edge absorption spectroscopy (XANES) with a tabletop high-harmonic extreme ultraviolet (XUV) spectrometer. Visible-light photoexcitation of $Fe(tpy)_2(BF_4)_2$ (where tpy = terpyridine) creates a metal-to-ligand charge transfer (MCLT) state that decays in 170 fs to a metal-centered triplet state (^{3}MC), followed by 38 fs decay by intersystem crossing to a metal-centered quintet (^{5}MC). Coherent oscillations on the ^{5}MC surface are observed as a modulation in the XANES spectrum with a frequency of 103 cm^{-1} and a spectral shape that is characteristic of the symmetric Fe-N stretch. These dynamics and spectra are similar to those previously observed for $Fe(phen)_3^{2+}$ (phen = phenanthroline). In contrast, transient spectroscopy of $Fe[(4\text{-}CF_3)_2bpca]_2$ (bpca= bis(2-pyridylcarbonyl)amide) reveals a lower-frequency 42 cm^{-1} coherent oscillation. Ligand field multiplet calculations combined with *ab initio* ligand field theory identify this oscillation as a ligand bending mode, highlighting the ligand field sensitivity of M-edge XANES. The activation of different vibrational modes in $Fe(tpy)_2(BF_4)_2$ and $Fe[(4\text{-}CF_3)_2bpca]_2$ is explained by mapping their excited-state potential energy surfaces using density functional theory. In the latter complex, the nuclear trajectory follows initial expansion along the $Fe\text{-}N_{axial}$ coordinate until reaching the ^{3}MC/^{5}MC seam. After intersystem crossing, the quintet state is significantly displaced along the coordinate corresponding to the ligand rocking mode, which therefore dominates the subsequent trajectory.

Introduction

The ability to convert light into electrical and chemical energy is a promising solution to deal with increasing global energy needs. Accomplishing this goal with molecular photosensitizers requires long-lived excited states, on the order of hundreds of nanoseconds for solution-phase bimolecular photochemistry. Many systems that meet this requirement are based upon second- and third-row transition metals such as Ru^{II} and Ir^{III},[1,2] but these elements are not abundant enough to be used for wide-scale light harvesting applications. For this reason, recent efforts have focused on creating first-row transition metal complexes with long-lived excited states.[3,4] Of first-row transition metals, isoelectronic d^6 complexes such as $Fe(bpy)_3^{2+}$ might be expected to have properties similar to those of $Ru(bpy)_3^{2+}$, but unfortunately the lifetime of its MLCT state is ~100 fs vs. hundreds of nanoseconds for $Ru(bpy)_3^{2+}$.[5,6] The short lifetimes of Fe^{II} complexes arise from

the greater radial contraction of the d orbitals (vs. the valence s and p orbitals), thereby causing the d orbitals to overlap less with ligand bonding orbitals and reducing the ligand field strength.[7] The reduced ligand field strength lowers the energy of the high-spin metal-centered (MC) excited states, so that they cross the MLCT state near the Franck-Condon region of the potential energy surface. The MLCT state therefore relaxes onto the MC surface on a femtosecond timescale, driving a structural distortion due to population of antibonding e_g orbitals.[8]

One common approach to increasing the MLCT lifetimes of Fe^{II} chromophores is to raise the energies of the MC states by employing strongly σ-donating / π-accepting ligands.[9–11] Using this method, MLCT lifetimes of up to 528 ps have been reported.[10] Other methods include using steric effects to produce high-spin Fe^{II} species with ^{5}MLCT excited states,[12] and tuning ligand orbital energies to increase the ligand character of the highest-occupied molecular orbitals (leading to increased covalency and/or HOMO inversion).[13–16] One less-commonly employed strategy – to displace or deform the excited state potential energy surface and thereby change the intersection points between the MLCT and ^{3,5}MC states – has been used to increase the lifetimes of Fe^{II} and Cr^{III} excited states by ~10-fold.[17,18] In both cases, the ligand cage was modified sterically in such a way to inhibit nuclear motion along the reaction coordinate associated with conversion to the MC states. We recently showed that restricting expansion along the Fe-ligand symmetric stretch coordinate using a macrocyclic ligand resulted in a reasonably long MLCT lifetime of 1.25 ns.[19]

Modifying the intersystem crossing (ISC) reaction coordinate from the typical isotropic expansion of iron-ligand bonds is an additional strategy that has been used to tune the excited-state properties of Fe^{II} chromophores. This concept has been previously used to extend the ^{5}MC state lifetime in Fe^{II} polypyridyl complexes, the prototypical example being the increased ^{5}MC lifetime of $Fe(tpy)_2^{2+}$ compared to that of $Fe(bpy)_3^{2+}$.[20] By using a bis-meridional coordination geometry, an additional ligand bending coordinate is involved in ISC, typically described in terms of a change in the N-N-N angle defined by the three nitrogen atoms within a single ligand. This symmetric in-plane bending mode (which has been called a rocking motion but which is perhaps better described as a pinching motion with respect to the metal center) has been previously identified in computational studies as an important mode during ultrafast ISC.[21]

Further modifications of the bis-meridional framework can make the ISC reaction coordinate depart further from the fully symmetric stretch and lead to new, interesting dynamics. Previous studies of the ultrafast dynamics of the 2,6-bis(2-carboxypyridyl)pyridine complex $Fe(dcpp)_2^{2+}$ showed that de-excitation back to the ground state was ~20x slower than in $Fe(tpy)_2^{2+}$.[22] X-ray scattering experiments showed that the Fe-N_{ax} bond lengths in $Fe(dcpp)_2^{2+}$ increased by only +0.09 Å in the ^{5}MC state in comparison to a more typical +0.23 Å expansion of the Fe-N_{eq} bonds, likely arising from an increased flexibility of the ligand rocking during low-spin (LS) to high-spin (HS) conversion.[23] Although the increase in the ground state recovery rate was not attributable to relaxation from a ^{3}MC state (and instead, from a ^{5}MC state with a near zero activation energy barrier), discovery of an anisotropic bond expansion of the ligand cage gives prospective methods for tuning excited state behavior.

With this strategy in mind, we herein used ultrafast M-edge X-ray absorption near edge structure (XANES) to probe how changes along the ligand rocking coordinate in bis-meridional iron(II) complexes can lead to changes in the photoinduced spin crossover (SCO) dynamics on the femtosecond timescale. We have previously shown that M-edge XANES is sensitive to changes in oxidation state, spin-state, and the ligand coordination environment, making it a powerful tool to observe electronic states involved in ultrafast SCO along with vibrational coherences which modify Fe-ligand bonds.[24,25] This technique coupled with computational methods shows that the ISC reaction coordinate can be modified to near-directly with the ligand rocking coordinate, and can be experimentally observed by changes in the spectral component of observed vibrational coherences.

Experimental

Sample preparation and M-edge XANES. The synthesis and characterization of Fe[(4-CF_3)$_2$bpca]$_2$ are described in the Supporting Information. Films of Fe[(4-CF_3)$_2$bpca]$_2$ were deposited by thermal evaporation at 10^{-5} Torr and above 200 °C onto 50 nm Si_3N_4 membranes. Films of Fe(tpy)$_2$(BF_4)$_2$ were produced by spin coating a concentrated solution of Fe(tpy)$_2$(BF_4)$_2$ in MeCN on a ~200 nm thick film of polyvinyl chloride (PVC).[26] The approximate thickness of each film was 100 nm. A description of the transient $M_{2,3}$-edge XANES spectrometer and data processing can be found elsewhere.[25] The spectrometer resolution during the experiment was roughly 0.3 eV measured by fitting atomic transitions of Xe^+ and Kr^+. Excitation pulses of ~2 µJ centered at 525 or 575 nm were used for Fe[(4-CF_3)$_2$bpca]$_2$ and Fe(tpy)$_2^{2+}$, respectively, corresponding to a pump fluence of ~1.5 mJ/cm^2.

DFT Calculations. All density-functional theory (DFT) and time-dependent DFT (TDDFT) calculations were carried out using QCHEM (v5.0.2).[27] DFT and TDDFT calculations employed the B3LYP* functional[28] (a variant of the traditional B3LYP functional[29,30] incorporating 20% of exact exchange, *vs.* 15% in the original formulation) and used the resolution-of-identity (RI) approximation for the Coulomb and Hartree-Fock exchange integrals (RIJK). The *def*2-TZVP[31,32] basis set of Ahlrichs and Weigend was used throughout. An SCF convergence criterion of 1.0×10^{-7} a.u. was used in all calculations; convergence criteria of 1.0×10^{-6} and 3.0×10^{-5} a.u. were used for the energy change and RMS gradient, respectively, in all geometry optimizations. The proper convergence of all geometry optimizations to real minima was verified by vibrational frequency inspection.

CASSCF + NEVPT2 Calculations. All complete active space self-consistent field (CASSCF) and *N*-electron valence 2nd-order perturbation theory (NEVPT2) calculations were carried out using ORCA (v4.2.1).[33–35] As recommended by Pierloot and Vancoillie,[36] the largest CASSCF active space comprised ten electrons distributed over twelve orbitals: five of A symmetry ($d_{x^2-y^2}$ and $2d_{x^2-y^2}$; σ_{z^2} and $\sigma^*_{z^2}$; $2d_{z^2}$), three of B_1 symmetry (σ_{xy} and σ^*_{xy}; $2d_{xy}$), and two of each B_2 (d_{xz} and $2d_{xz}$), and B_3 (d_{yz} and $2d_{yz}$) symmetry. State-averaging was carried out over the four lowest-energy singlet MC states (one of each A, B_1, B_2, and B_3 symmetry), the six lowest-energy

triplet MC states (two of each B_1, B_2, and B_3 symmetry), and the three lowest-energy quintet MC states (one of each B_1, B_2, and B_3 symmetry) with equal weighting being given to all states. These calculations are denoted SA13-CASSCF(10,12) hereafter. A minimal truncated CASSCF active space comprising six electrons distributed over five orbitals – two of A symmetry ($d_{x^2-y^2}$ and $\sigma^*_{z^2}$) and one of each B_1 (σ^*_{xy}), B_2 (d_{xz}), and B_3 (d_{yz}) symmetry – was also constructed by omission of the two lowest-energy occupied orbitals (both of A symmetry) and the additional "double" shell of five *d* orbitals. The same state-averaging scheme was used. These calculations are denoted SA13-CASSCF(6,5) hereafter. All calculations used the RI approximation for the Coulomb and Hartree-Fock exchange integrals (RIJK). The *def*2-TZVP[31,32] basis set of Ahlrichs and Weigend was used throughout. Calculations were carried out using B3LYP*/*def*2-TZVP geometries. An SCF convergence criterion of 1.0×10^{-7} a.u. was used in all calculations. See Supporting Information for more details.

Ab Initio Ligand Field Theory Calculations

All *ab initio* ligand field theory (AILFT) calculations were carried out using ORCA (v4.1.0).[33–35] The SA13-CASSCF(6,5) calculations were used as the basis for the AILFT. Two coordinates were considered; an Fe-N stretching coordinate connecting the optimized singlet (^{1}A) and quintet ($^5B_2$) geometries, and a ligand rocking coordinate obtained from DFT vibrational frequency analysis at the $^5B_2$ minimum-energy geometry. Three points were interpolated in each direction from the minimum-energy geometry along each coordinate (yielding seven points in total). At each point, ligand field one-electron eigenfunctions were calculated by AILFT to determine the ligand field parameters 10Dq, Ds, and Dt; ligand field parameters between the sampled points were approximated *via* fitting each parameter with a quadratic function.

Ligand Field Multiplet Simulations

Simulations of Fe *M*-edge XAS spectra were carried out using ligand field multiplet (LFM) theory using CTM4XAS.[37] LFM theory models the X-ray absorption site in terms of a parametric Hamiltonian containing atomic terms and a molecular crystal field term. The atomic terms include electron-electron repulsion and exchange terms under the Hartree-Fock approximation using tabulated Slater integrals that can be scaled to account for electron delocalization. The molecular crystal field term is purely electrostatic, and crystal field strengths are assumed to be equivalent in the electronic ground state and the core-hole state. Using LFM theory, correlation diagrams were constructed by simulating the Fe *M*-edge XAS spectra along the N-N-N rocking coordinate in steps of 0.5° and along the Fe-N_{ax} (symmetric) stretching coordinate in steps of 0.01 Å. Heatmaps were generated *via* linear interpolation onto a finer grid (0.05 °; 0.001 Å spacing) and broadened with a two-dimensional Gaussian filter with σ of 5 points along both axes (step size 10 meV, 0.1° / 0.005 A for the axes). Simulated Fe *M*-edge XAS spectra shown alongside the correlation diagrams display intrinsic lifetime broadening and a Fano lineshape (q = 3.5) to account for electronically-excited states decaying through a super Coster-Kronig Auger pathway.

Results

Our study focuses on the dynamics of two bis-meridional Fe^{II} complexes (**Figure 1**): The first molecule is $Fe(tpy)_2^{2+}$, a prototypical bis-meridional Fe^{II} complex that has been the subject of many experimental and theoretical investigations.[4,20,21,38,39] The second molecule is iron(II) bis[4-(trifluoromethyl)-2-pyridylcarbonyl)amide ($Fe[(CF_3)_2bpca]_2$), which is very similar to $Fe(tpy)_2^{2+}$ except that the central pyridine ring has been replaced with an amide group. This modification significantly increases the flexibility of the ligand along the internal rocking coordinate, and several differences in the photophysics and excited state structures arise from this difference.

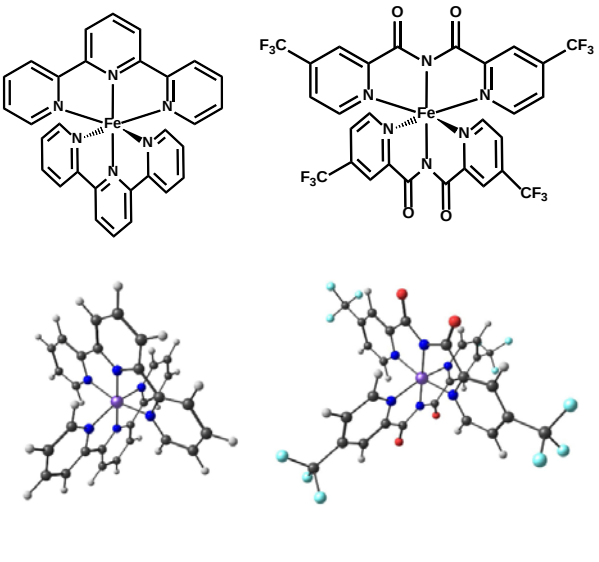

Figure 1: Schematic and optimized structure of $Fe(tpy)_2^{2+}$ (A,B) and $Fe[(CF_3)_2bpca]_2$ (C,D)

Compared to the geometry of the excited ^{1}MC state of $Fe(tpy)_2^{2+}$, in which the Fe-N_{ax} and Fe-N_{eq} distances are distinctly different (**Table 1**), the DFT-optimized ^{1}MC geometry of $Fe[(CF_3)_2bpca]_2$ is much more nearly octahedral: the Fe-N_{ax} and Fe-N_{eq} bond distances are equal within 0.02 Å, and the N-N-N angle is distorted by only 8.5° from the ideal O_h value of 90°. In contrast, in the ^{5}MC geometry the Fe-N bond lengths and N-N-N angle of the two complexes are similar: in both compounds the Fe-N_{ax} distance is about 0.09 Å shorter than the Fe-N_{eq} distance. Thus, along the ^{1}MC to ^{5}MC SCO reaction coordinate, the Fe-N distances in $Fe(tpy)_2^{2+}$ increase isotropically by about 0.23 Å, but the Fe-N bond lengths for $Fe[(4\text{-}CF_3)_2bpca]_2$ expand anisotropically by 0.15 Å for Fe-N_{ax} vs. 0.22 Å for Fe-N_{eq}. The ISC reaction coordinate is also attended by a larger change of the N-N-N angle in $Fe[(4\text{-}CF_3)_2bpca]_2$ compared to $Fe(tpy)_2^{2+}$ (+7.8° vs +5.4°). One would therefore expect a larger excitation of the ligand rocking mode in $Fe[(CF_3)_2bpca]_2$.

Table 1: Calculated Fe-N bond lengths of $Fe(tpy)_2^{2+}$ and $Fe[(CF_3)_2bpca]_2$ in their optimized singlet and quintet geometries

	$Fe(tpy)_2^{2+}$		$Fe[(CF_3)_2bpca]_2$	
	$^1A_1$	^5E	$^1A_1$	$^5B_2$
*r*Fe–N_{ax}	1.91	2.16	1.97	2.12
*r*Fe–N_{eq}	2.02	2.24	1.99	2.21

Transient M-edge XANES of $Fe(tpy)_2^{2+}$:

The femtosecond dynamics of $Fe(tpy)_2^{2+}$ were measured by exciting with a 35 fs pulse centered at 575 nm and probing with a 15 fs broadband XUV probe. An overview of the transient M-edge response for $Fe(tpy)_2^{2+}$ is shown in the heatmap in Figure 2A, and the data are interpreted in light of a previous femtosecond M-edge XANES study of $Fe(phen)_3^{2+}$.[25] During the first 50 fs there is a weak, broad absorption from 53.5-62.0 eV, indicating initial population of an MLCT excited state. Within the first 100 fs, a small feature arises at 66 eV which is delayed from t_0, then decays within 200 fs. This feature was previously identified as a fingerprint for a ^{3}MC intermediate state.[25] Within this same timescale, a bleach appears above 65 eV along with two strong positive features at 55.5 and 57.2 eV, signaling conversion to the ^{5}MC state (Figure 2B). Over the next 500 fs, coherent oscillations of the positive features are observed with a period of ~325 fs.

The frequency and spectrum of the oscillations observed on the quintet surface provide a fingerprint for the nuclear motion in the first coordination shell of the Fe atom. . The spectra were fit to a three-state ^{1,3}MLCT → ^{3}MC → ^{5}MC kinetic model with a damped oscillation on the ^{5}MC state. The resulting component spectra are shown in Figure 2D;the derived time constants for the

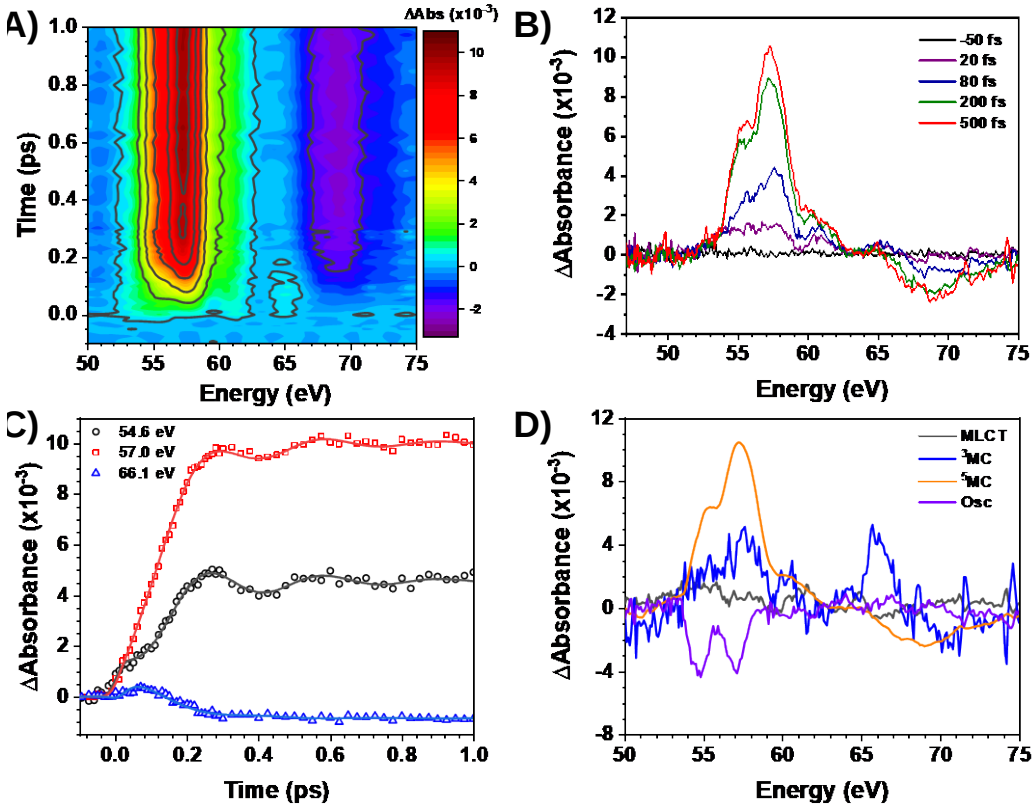

Figure 2: A) Contour plot of transient M-edge XANES spectra of $Fe(tpy)_2^{2+}$. B) Selected transient spectra at selected times. C) Experimental kinetic slices at selected energies (open symbols) with reconstructed kinetic traces from the global fit (solid lines). D) Component spectra from the MLCT → ^{3}MC → ^{5}MC + damped oscillation global fit.

three states and the damped oscillation are τ_{MLCT} = 106 ± 10 fs, τ_{3MC} = 38 ± 10 fs, τ_{osc} = 324 ± 12 fs, and τ_{damp} = 315 ± 15 fs. Overall, the resulting component spectra are similar to those seen for $Fe(phen)_3^{2+}$, for which we previously measured τ_{MLCT} = 170 ± 9 fs, τ_{3MC} = 39 ± 6 fs, τ_{osc} = 249 ± 9 fs, and τ_{damp} = 630 ± 330 fs. As will be discussed below, the shape of the oscillation spectrum (in this case two peaks at 54.6 and 57.1 eV that start negative when the wavepacket is launched) is a fingerprint of the specific vibrational mode that is activated by ISC.

Transient M-edge XANES of $Fe[(CF_3)_2bpca]_2$:

An overview of the transient response of $Fe[(CF_3)_2bpca]_2$ after 525 nm excitation is shown in Figure 3A. Due to fluctuations in the probe spectrum, which cause sharp artifacts to appear in the transient data, the energy axis was binned into 0.5 eV segments (vs. the 0.1 eV binning used for $Fe(tpy)_2^{2+}$. Owing to the broad linewidths of M-edge transitions, we considered this to be an acceptable compromise. Overall, the dynamics are similar to those seen in $Fe(tpy)_2^{2+}$. Within the first 50 fs, a weak excited-state absorption spanning from 54-65 eV is observed with a small bleach at 59.0 eV. As with $Fe(tpy)_2^{2+}$, this transient spectrum is assigned to the ^{3}MLCT state. Between 50

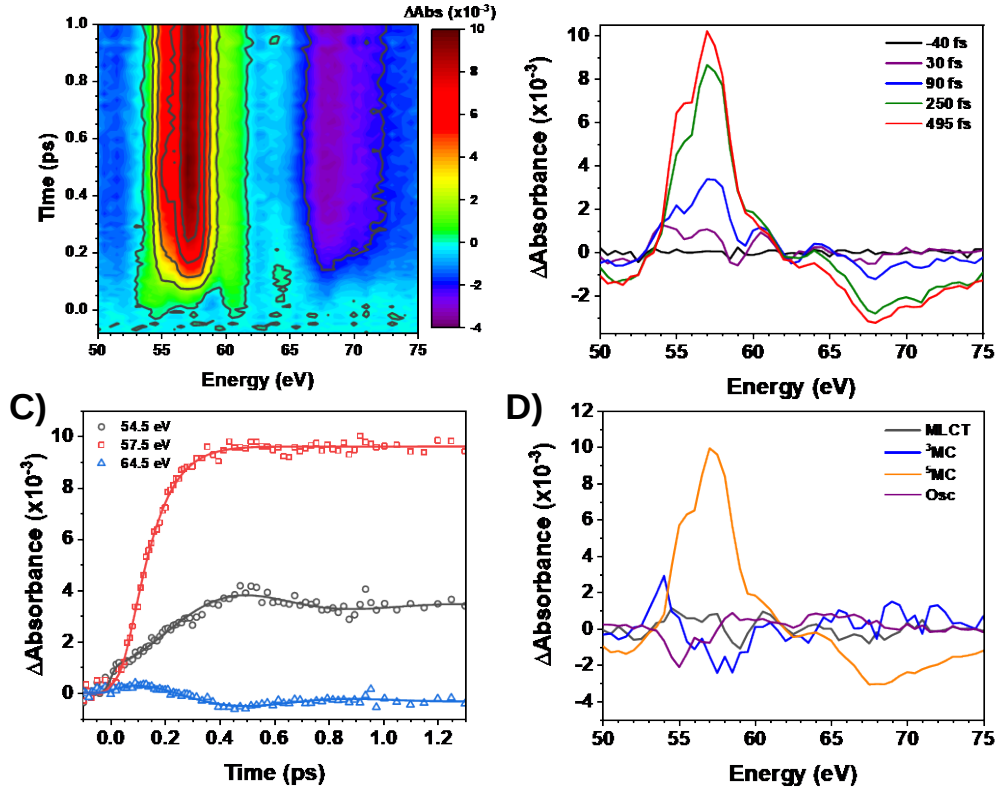

Figure 4: A) Contour plot of transient M-edge XANES spectra of $Fe[(CF_3)_2bpca]_2$. B) Selected transient spectra at selected times. C) Experimental kinetic slices at selected energies (open symbols) with reconstructed kinetic traces from the global fit (solid lines). D) Component spectra from the MLCT → ^{3}MC → ^{5}MC + damped oscillation global fit.

and 150 fs, the ^{3}MC feature at 64.5 eV first grows in, and then decays away. In the first few hundred femtoseconds, absorption features at 55.5 and 57.0 eV grow along with a broad bleach centered at 68.0 eV. Select spectra are shown in Figure 3B to highlight the trends described above. An oscillation is observed in the 54.5 eV and 64.5 eV traces, but with a much longer period than in $Fe(tpy)_2^{2+}$ (Figure 3C).

This transient data set measured for $Fe[(CF_3)_2bpca]_2$ was also fit to the same three-state global model with a damped oscillation used for $Fe(tpy)_2^{2+}$. The resulting component spectra are shown in Figure 3D, and the deduced time constants are $\tau_{MLCT} = \tau_{3MC} = 66 \pm 1$ fs, $\tau_{osc} = 703 \pm 16$ fs and $\tau_{damp} = 321 \pm 80$ fs. Unfortunately, this fitting algorithm fails to recover a ^{3}MC spectrum that matches the experimental slices in the 50-150 fs range, likely due to the similarity between the lifetimes of the ^{3}MLCT and ^{3}MC states. As is discussed in detail in the Supporting Information, a reasonable ^{3}MC spectrum similar to that of $Fe(tpy)_2^{2+}$ and $Fe(phen)_3^{2+}$ can be obtained by imposing constraints on the fit.

The spectrum of the coherent oscillation seen for $Fe[(CF_3)_2bpca]_2$ consists of a main negative feature at 55.0 eV, slight negative feature at 57.0 eV and a broad positive feature past 58 eV. The oscillation period of 785 ps (42.5 cm^{-1}) is also much slower than seen in $Fe(tpy)_2^{2+}$ and $Fe(phen)_3^{2+}$. A simple normal mode analysis of $Fe[(4\text{-}CF_3)_2bpca]_2$ shows that there is a ligand rocking mode at a similar frequency (46.0 cm^{-1}), which is expected to be a large component of the ISC reaction coordinate owing to the greater lengthening the Fe-N_{eq} bonds vs. the Fe-N_{ax} bond. As shown in the Supporting Information, the spectrum of the oscillation can also be identified by subtracting the transient spectra averaged from 425-525 fs from the spectrum after 1 ps.

Simulations of vibrational component spectra:

To obtain further insight into the origin of the oscillatory component spectrum observed for $Fe[(CF_3)_2bpca]_2$, we carried out AILFT calculations along two motions of the $^5B_2$ state likely to be excited by the ultrafast ISC process: the ligand rocking coordinate (obtained from DFT vibrational frequency analysis at the $^5B_2$ minimum-energy geometry), and an Fe-N breathing mode (i.e., the stretching coordinate connecting the optimized singlet (^1A) and quintet ($^5B_2$) geometries). The calculated M-edge difference spectra for the $^5B_2$ state along both nuclear coordinates are shown in Figure 4. Expected oscillatory component spectra are also shown in this figure, calculated by subtracting spectra at the two extremes of motion (compressed vs. expanded Fe-N distances). The positions chosen for the difference spectra were both 0.5 eV higher in energy than the minimum geometry.

Simulations for motion along the breathing coordinate contains two negative features at 55 and 57 eV, as was seen in $Fe(tpy)_2^{2+}$ and $Fe(phen)_3^{2+}$. A simulation for motion along the ligand rocking coordinate contains a negative feature at 55 eV, a small positive feature at 56 eV, and a broad positive feature past 58 eV. This rocking simulation is an excellent match for the experimental oscillation component spectrum of $Fe[(CF_3)_2bpca]_2$. In view of the match in both the spectral fingerprint and the vibrational frequency, we conclude that the oscillations in this molecule correspond to motion along the ligand rocking coordinate and not the breathing coordinate.

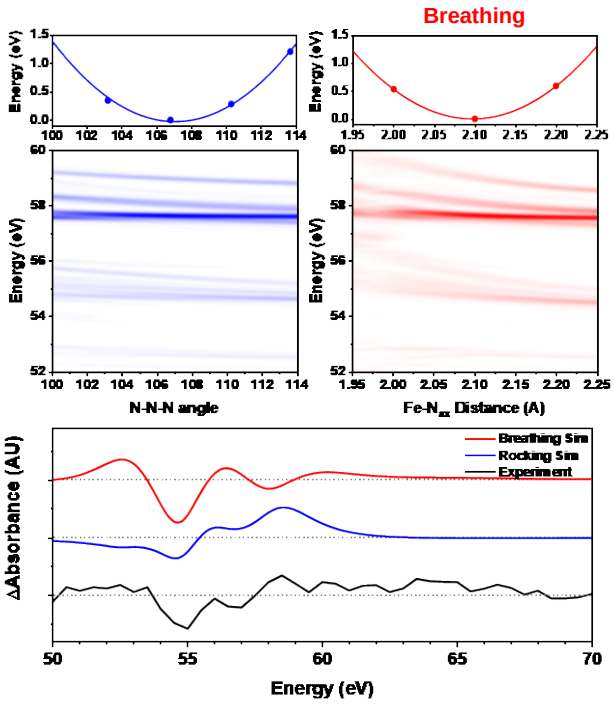

Figure 5: Top: Calculated energies of the quintet state along both rocking and breathing modes using SA-CASSCF(6,5) (points) shown with a quadratic fit (line). Middle: Simulated stick spectra along both modes using ligand field parameters extracted from AILFT calculations. Bottom) Simulated difference spectra along the rocking and breathing coordinates compared to the experimental modulation of the quintet spectrum. The simulated spectra are calculated by taking a difference between compressed and expanded points 0.5 eV higher in energy than the quintet minimum geometry.

Discussion

The different behavior of Fe[$(CF_3)_2$bpca] vs. $Fe(tpy)_2^{2+}$ and $Fe(phen)_3^{2+}$ is similar in some respects to that seen in a study of photoinduced electron transfer in an iron perylene diimide complex, in which there were two distinct vibrational signatures in the optical transient absorption spectrum: a high-frequency mode specific to the reactant, and a low-frequency mode specific to the product.[40] They concluded that the dynamics were consistent with the wavepacket on the product surface originating from a structure displaced from the equilibrium geometry along the low-frequency mode.

The qualitative difference in vibrational wavepacket dynamics between the two bis-meridional complexes $Fe(tpy)_2(BF_4)_2$ and Fe[$(4\text{-}CF_3)_2$bpca]$_2$ reflects differences in the initial position and/or momentum on the ^{5}MC surface where the wavepacket is launched. In $Fe(tpy)_2^{2+}$, the wavepacket launched on the ^{5}MC surface has a signature and frequency consistent with a nearly symmetric change in all Fe-N bond lengths, and therefore suggests the nuclear trajectory of the complex that produces the ^{5}MC state is an isotropic expansion of metal-ligand bonds. Contrastingly, the wavepacket launched in Fe[$(CF_3)_2$bpca]$_2$ has a frequency and signature consistent with motion along the ligand rocking mode, and therefore suggests the wavepacket is launched at a position displaced primarily along this coordinate. Therefore, we suspect the nuclear trajectory likely involves an initial expansion along the Fe-N_{ax} bonds before reaching the quintet surface, followed by motion along the ligand rocking mode.

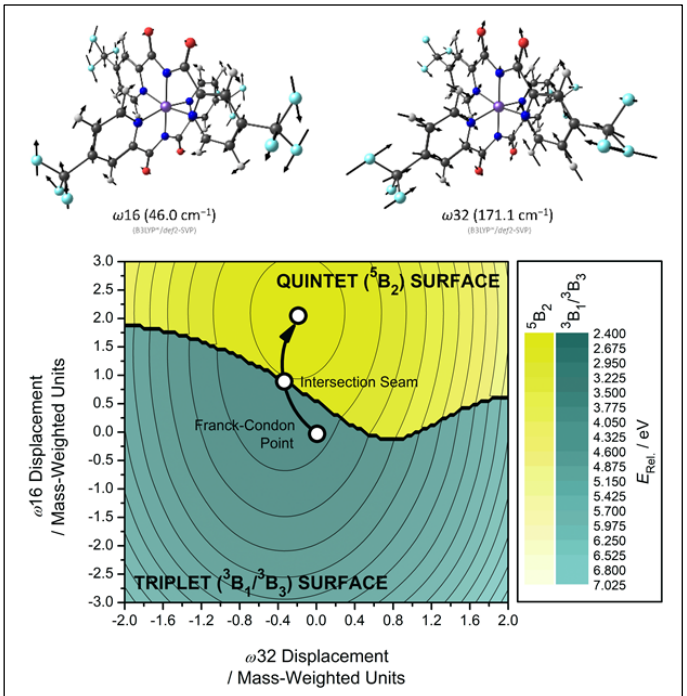

Figure 6: Top) Vector diagrams of the two key low-frequency ground-state normal modes of Fe[$(CF_3)_2$bpca]$_2$, ω16 (46.0 cm^{-1}) and ω32 (171.1 cm^{-1}), at the B3LYP*/def2-TZVP level. Bottom) Two-dimensional potential energy surfaces of the lowest-lying triplet ($^3B_1/^3B_3$) and quintet ($^5B_2$) MC states along the ω16 (46.0 cm^{-1}) and ω32 (171.1 cm^{-1}) ground-state normal mode coordinates of Fe[$(CF_3)_2$bpca]$_2$. Energies are plot relative to the ^{1}A-state (ground-state) energy of the ^{1}A minimum-energy geometry at zero displacement. The potential energy surface shown is the highest-energy surface at that coordinate (e.g. population can transfer from the higher-energy $^3B_1/^3B_3$ surfaces to the lower-energy $^5B_2$ surface along ω16); the black line demarks the intersection of the $^3B_1/^3B_3$ and $^5B_2$ potential energy surfaces where the energetic ordering of the surfaces interchanges.

This hypothesis is supported by nature of the DFT(B3LYP*)-calculated intersection seam for Fe[$(CF_3)_2$bpca]$_2$ between the lowest ^{3}MC and ^{5}MC surfaces along the two vibrational modes most involved along the SCO reaction coordinate: the ligand rocking mode (ω16) which changes Fe-N_{eq} bond lengths and a breathing mode which primarily changes Fe-N_{ax} bond lengths (ω32). As expected from previously described differences in the

^{1}MC and ^{5}MC geometries, the primary nuclear displacement from the Frank-Condon region to the ^{5}MC minimum energy geometry is along the ligand rocking mode (Figure 5). Of equal importance, the minimum energy of the intersection seam compared to the ^{5}MC minimum geometry is displaced almost solely along ω16. Therefore, if arrival to the ^{5}MC state occurs close to the minimum energy of the intersection seam, the observed vibrational wavepacket would propagate primarily along ω16.

Notably, the ^{5}MC lifetime of Fe[$(CF_3)_2$bpca]$_2$ is 48 ± 1 ns, which is an order of magnitude longer than that of Fe(tpy)$_2^{2+}$ (see Supporting Information). Although these two measurements were carried out in different solvents (dichloromethane vs. acetonitrile), and ^{5}MC lifetimes can be somewhat solvent-dependent,[41] the increase in the ^{5}MC lifetime of Fe[$(CF_3)_2$bpca]$_2$ is too large to be attributed to this effect. Instead, the lengthening is likely due primarily to a weakening of the ligand field strength, which increases the energy barrier between ^{5}MC and ^{1}MC states.[42] Modifications of this ligand platform to reduce the ligand field strength even more, therefore, could lead to further increases in the ^{5}MC lifetime.[43]

Conclusion

We have observed a substantial difference in the spin crossover photodynamics of bis-meridional iron(II) complexes upon modifying the ligand and its vibrational frequencies. The difference in dynamics during photoinduced ISC arises from changes in the reaction coordinate from a symmetric expansion of Fe-N bonds seen for Fe(tpy)$_2^{2+}$ to an anisotropic expansion primarily along Fe-N_{eq} bond axes seen for Fe[$(CF_3)_2$bpca]$_2$. The results show that time-resolved femtosecond M-edge XANES spectra provide two distinct signatures – the oscillation frequency observed in the time domain as well as the modulation footprint observed in the energy domain. Changes in the M-edge spectra caused by slight changes in coordination geometry, coupled with AILFT and LFM simulations, provide a powerful technique to identify nuclear motion coupled with electron dynamics. This combination of experiment and theory can be used to map out key reaction coordinates during photophysical processes. This technique is complementary to other ultrafast techniques such as X-ray solution scattering[44] and impulsive vibrational spectroscopy,[45] and is reminiscent of nuclear resonant vibrational spectroscopy[46] in that it selectively probes vibrational modes involving the metal center.

For Fe[$(CF_3)_2$bpca]$_2$, the intersection region between the ^{3}MC and ^{5}MC states changes significantly compared to Fe(tpy)$_2^{2+}$, but further ligand modifications could also change the intersection region between MLCT and MC states to enhance MLCT lifetimes. The ability to change the reaction coordinate of spin-crossover by changing ligand vibrational modes could provide a powerful tool alongside increasing ligand field strength to controlling the dynamics of Fe^{II} photosensitizers, and a powerful tool in general for controlling photophysical processes.

Supplementary Material

Synthesis and characterization of $Fe[(CF_3)_2bpca]_2$, details on calculations, further investigation of the 3MC spectrum, and fs/ns optical transient absorption spectroscopy.

Acknowledgements

J.V.W. and G.S.G. thank the National Science Foundation for support of this work (CHE 21-02376). T.J.P acknowledges EPSRC through projects EP/W008009/1, EP/X035514/1 and EP/X026973/1 for funding. We thank Andrew King for help with the ligand synthesis, and Dr. Rafael López-Arteaga and Prof. Emily Weiss for collecting the nanosecond transient absorption data.

Author Declarations

Conflict of Interest

The authors have no conflicts to disclose.

Author Contributions:

Ryan T. Ash: Investigation (equal), Writing – original draft (lead), Formal analysis (lead), Conceptualization (supporting), Methodology (lead)

Kaili Zhang: Investigation (equal), Writing – review & editing (supporting), Formal analysis (supporting), Conceptualization (lead)

Conor D. Rankine: Investigation (supporting), Writing – review & editing (supporting), Formal analysis (supporting)

Justin T. Malme: Investigation (supporting), Writing – review & editing (supporting)

Thomas J. Penfold: Writing – review & editing (equal), Funding Acquisition (supporting), Conceptualization (supporting), Supervision (equal)

Gregory S. Girolami: Writing – review & editing (equal), Funding Acquisition (supporting), Supervision (equal)

Josh Vura-Weis: Writing – review & editing (equal), Funding Acquisition (lead), Conceptualization (supporting), Supervision (equal)

Data Availability

All data is available at reasonable request.

References

(1) Prier, C. K.; Rankic, D. A.; MacMillan, D. W. C. Visible Light Photoredox Catalysis with Transition Metal Complexes: Applications in Organic Synthesis. *Chem. Rev.* **2013**, *113* (7), 5322–5363.

(2) Nazeeruddin, M. K.; Kay, A.; Rodicio, I.; Humphry-Baker, R.; Mueller, E.; Liska, P.; Vlachopoulos, N.; Graetzel, M. Conversion of Light to Electricity by Cis-X2bis(2,2'-Bipyridyl-4,4'-Dicarboxylate)Ruthenium(II) Charge-Transfer Sensitizers (X = Cl-, Br-, I-, CN-, and SCN-) on Nanocrystalline Titanium Dioxide Electrodes. *J. Am. Chem. Soc.* **1993**, *115* (14), 6382–6390.

(3) Wenger, O. S. Is Iron the New Ruthenium? *Chem. - A Eur. J.* **2019**, *25* (24), 6043–6052.

(4) Liu, Y.; Harlang, T.; Canton, S. E.; Chábera, P.; Suárez-Alcántara, K.; Fleckhaus, A.; Vithanage, D. A.; Göransson, E.; Corani, A.; Lomoth, R.; Sundström, V.; Wärnmark, K. Towards Longer-Lived Metal-to-Ligand Charge Transfer States of Iron(Ii) Complexes: An N-Heterocyclic Carbene Approach. *Chem. Commun.* **2013**, *49* (57), 6412–6414.

(5) Bergkamp, M. A.; Chang, C. K.; Netzel, T. L. Quantum Yield Determinations for Subnanosecond-Lived Excited States and Photoproducts: Applications to Inorganic Complexes and Photosynthetic Models. *J. Phys. Chem.* **1983**, *87* (22), 4441–4446.

(6) Gawelda, W.; Cannizzo, A.; Pham, V. T.; Van Mourik, F.; Bressler, C.; Chergui, M. Ultrafast Nonadiabatic Dynamics of $[Fe^{II}(Bpy)3]2+$ in Solution. *J. Am. Chem. Soc.* **2007**, *129* (26), 8199–8206.

(7) McCusker, J. K. Electronic Structure in the Transition Metal Block and Its Implications for Light Harvesting. *Science* **2019**, *363* (6426), 484–488.

(8) Sousa, C.; de Graaf, C.; Rudavskyi, A.; Broer, R.; Tatchen, J.; Etinski, M.; Marian, C. M. Ultrafast Deactivation Mechanism of the Excited Singlet in the Light-Induced Spin Crossover of $[Fe(2,2'\text{-Bipyridine})_3]^{2+}$. *Chem. - A Eur. J.* **2013**, *19* (51), 17541–17551.

(9) Liu, Y.; Persson, P.; Sundström, V.; Wärnmark, K. Fe N-Heterocyclic Carbene Complexes as Promising Photosensitizers. *Acc. Chem. Res.* **2016**, *49* (8), 1477–1485.

(10) Chábera, P.; Kjaer, K. S.; Prakash, O.; Honarfar, A.; Liu, Y.; Fredin, L. A.; Harlang, T. C. B.; Lidin, S.; Uhlig, J.; Sundström, V.; Lomoth, R.; Persson, P.; Wärnmark, K. Fe^{II} Hexa N-Heterocyclic Carbene Complex with a 528 Ps Metal-To-Ligand Charge-Transfer Excited-State Lifetime. *J. Phys. Chem. Lett.* **2018**, *9* (3), 459–463.

(11) Chábera, P.; Fredin, L. A.; Kjær, K. S.; Rosemann, N. W.; Lindh, L.; Prakash, O.; Liu, Y.; Wärnmark, K.; Uhlig, J.; Sundström, V.; Yartsev, A.; Persson, P. Band-Selective Dynamics in Charge-Transfer Excited Iron Carbene Complexes. *Faraday Discuss.* **2019**, *216*, 191–210.

(12) Fatur, S. M.; Shepard, S. G.; Higgins, R. F.; Shores, M. P.; Damrauer, N. H. A Synthetically Tunable System To Control MLCT Excited-State Lifetimes and Spin States in Iron(II) Polypyridines. *J. Am. Chem. Soc.* **2017**, *139* (12), 4493–4505.

(13) Larsen, C. B.; Braun, J. D.; Lozada, I. B.; Kunnus, K.; Biasin, E.; Kolodziej, C.; Burda,

C.; Cordones, A. A.; Gaffney, K. J.; Herbert, D. E. Reduction of Electron Repulsion in Highly Covalent Fe-Amido Complexes Counteracts the Impact of a Weak Ligand Field on Excited-State Ordering. *J. Am. Chem. Soc.* **2021**, *143* (49), 20645–20656.

(14) Sinha, N.; Yaltseva, P.; Wenger, O. S. The Nephelauxetic Effect Becomes an Important Design Factor for Photoactive First-Row Transition Metal Complexes. *Angew. Chemie - Int. Ed.* **2023**, *62* (30), e202303864.

(15) Braun, J. D.; Lozada, I. B.; Kolodziej, C.; Burda, C.; Newman, K. M. E.; van Lierop, J.; Davis, R. L.; Herbert, D. E. Iron(Ii) Coordination Complexes with Panchromatic Absorption and Nanosecond Charge-Transfer Excited State Lifetimes. *Nat. Chem.* **2019**, *11* (12), 1144–1150.

(16) Mukherjee, S.; Torres, D. E.; Jakubikova, E. HOMO Inversion as a Strategy for Improving the Light-Absorption Properties of Fe(Ii) Chromophores. *Chem. Sci.* **2017**, *8* (12), 8115–8126.

(17) Schrauben, J. N.; Dillman, K. L.; Beck, W. F.; Mc Cusker, J. K. Vibrational Coherence in the Excited State Dynamics of Cr(Acac)3: Probing the Reaction Coordinate for Ultrafast Intersystem Crossing. *Chem. Sci.* **2010**, *1* (3), 405–410.

(18) Paulus, B. C.; Adelman, S. L.; Jamula, L. L. L.; McCusker, J. K. K. Leveraging Excited-State Coherence for Synthetic Control of Ultrafast Dynamics. *Nature* **2020**, *582* (7811), 214–218.

(19) Malme, J. T.; Clendening, R. A.; Ash, R.; Curry, T.; Ren, T.; Vura-Weis, J. Nanosecond Metal-to-Ligand Charge-Transfer State in an Fe(II) Chromophore: Lifetime Enhancement via Nested Potentials. *J. Am. Chem. Soc.* **2023**, *145* (11), 6029–6034.

(20) Hauser, A.; Enachescu, C.; Daku, M. L.; Vargas, A.; Amstutz, N. Low-Temperature Lifetimes of Metastable High-Spin States in Spin-Crossover and in Low-Spin Iron(II) Compounds: The Rule and Exceptions to the Rule. *Coord. Chem. Rev.* **2006**, *250* (13–14), 1642–1652.

(21) Nance, J.; Bowman, D. N.; Mukherjee, S.; Kelley, C. T.; Jakubikova, E. Insights into the Spin-State Transitions in [Fe(Tpy) 2] 2+ : Importance of the Terpyridine Rocking Motion. *Inorg. Chem.* **2015**, *54* (23), 11259–11268.

(22) Jamula, L. L.; Brown, A. M.; Guo, D.; McCusker, J. K. Synthesis and Characterization of a High-Symmetry Ferrous Polypyridyl Complex: Approaching the 5 T 2 / 3 T 1 Crossing Point for Fe II. *Inorg. Chem.* **2014**, *53* (1), 15–17.

(23) Britz, A.; Gawelda, W.; Assefa, T. A.; Jamula, L. L.; Yarranton, J. T.; Galler, A.; Khakhulin, D.; Diez, M.; Harder, M.; Doumy, G.; March, A. M.; Bajnóczi, É.; Németh, Z.; Pápai, M.; Rozsályi, E.; Sárosiné Szemes, D.; Cho, H.; Mukherjee, S.; Liu, C.; Kim, T. K.; Schoenlein, R. W.; Southworth, S. H.; Young, L.; Jakubikova, E.; Huse, N.; Vankó, G.; Bressler, C.; McCusker, J. K. Using Ultrafast X-Ray Spectroscopy To Address Questions in Ligand-Field Theory: The Excited State Spin and Structure of [Fe(Dcpp)2]2+. *Inorg. Chem.* **2019**, *58* (14), 9341–9350.

(24) Zhang, K.; Lin, M. F.; Ryland, E. S.; Verkamp, M. A.; Benke, K.; De Groot, F. M. F.;

Girolami, G. S.; Vura-Weis, J. Shrinking the Synchrotron: Tabletop Extreme Ultraviolet Absorption of Transition-Metal Complexes. *J. Phys. Chem. Lett.* **2016**, *7*, 3383–3387.

(25) Zhang, K.; Ash, R.; Girolami, G. S.; Vura-Weis, J. Tracking the Metal-Centered Triplet in Photoinduced Spin Crossover of $Fe(Phen)_3^{2+}$ with Tabletop Femtosecond M-Edge X-Ray Absorption Near-Edge Structure Spectroscopy. *J. Am. Chem. Soc.* **2019**, *141* (43), 17180–17188.

(26) Shari'ati, Y.; Vura-Weis, J. Polymer Thin Films as Universal Substrates for Extreme Ultraviolet Absorption Spectroscopy of Molecular Transition Metal Complexes. *J. Synchrotron Radiat.* **2021**, *28* (6), 1850–1857.

(27) Shao, Y.; Gan, Z.; Epifanovsky, E.; Gilbert, A. T. B.; Wormit, M.; Kussmann, J.; Lange, A. W.; Behn, A.; Deng, J.; Feng, X.; Ghosh, D.; Goldey, M.; Horn, P. R.; Jacobson, L. D.; Kaliman, I.; Khaliullin, R. Z.; Kuś, T.; Landau, A.; Liu, J.; Proynov, E. I.; Rhee, Y. M.; Richard, R. M.; Rohrdanz, M. A.; Steele, R. P.; Sundstrom, E. J.; Woodcock, H. L.; Zimmerman, P. M.; Zuev, D.; Albrecht, B.; Alguire, E.; Austin, B.; Beran, G. J. O.; Bernard, Y. A.; Berquist, E.; Brandhorst, K.; Bravaya, K. B.; Brown, S. T.; Casanova, D.; Chang, C.-M.; Chen, Y.; Chien, S. H.; Closser, K. D.; Crittenden, D. L.; Diedenhofen, M.; DiStasio, R. A.; Do, H.; Dutoi, A. D.; Edgar, R. G.; Fatehi, S.; Fusti-Molnar, L.; Ghysels, A.; Golubeva-Zadorozhnaya, A.; Gomes, J.; Hanson-Heine, M. W. D.; Harbach, P. H. P.; Hauser, A. W.; Hohenstein, E. G.; Holden, Z. C.; Jagau, T.-C.; Ji, H.; Kaduk, B.; Khistyaev, K.; Kim, J.; Kim, J.; King, R. A.; Klunzinger, P.; Kosenkov, D.; Kowalczyk, T.; Krauter, C. M.; Lao, K. U.; Laurent, A. D.; Lawler, K. V.; Levchenko, S. V.; Lin, C. Y.; Liu, F.; Livshits, E.; Lochan, R. C.; Luenser, A.; Manohar, P.; Manzer, S. F.; Mao, S.-P.; Mardirossian, N.; Marenich, A. V.; Maurer, S. A.; Mayhall, N. J.; Neuscamman, E.; Oana, C. M.; Olivares-Amaya, R.; O'Neill, D. P.; Parkhill, J. A.; Perrine, T. M.; Peverati, R.; Prociuk, A.; Rehn, D. R.; Rosta, E.; Russ, N. J.; Sharada, S. M.; Sharma, S.; Small, D. W.; Sodt, A.; Stein, T.; Stück, D.; Su, Y.-C.; Thom, A. J. W.; Tsuchimochi, T.; Vanovschi, V.; Vogt, L.; Vydrov, O.; Wang, T.; Watson, M. A.; Wenzel, J.; White, A.; Williams, C. F.; Yang, J.; Yeganeh, S.; Yost, S. R.; You, Z.-Q.; Zhang, I. Y.; Zhang, X.; Zhao, Y.; Brooks, B. R.; Chan, G. K. L.; Chipman, D. M.; Cramer, C. J.; Goddard, W. A.; Gordon, M. S.; Hehre, W. J.; Klamt, A.; Schaefer, H. F.; Schmidt, M. W.; Sherrill, C. D.; Truhlar, D. G.; Warshel, A.; Xu, X.; Aspuru-Guzik, A.; Baer, R.; Bell, A. T.; Besley, N. A.; Chai, J.-D.; Dreuw, A.; Dunietz, B. D.; Furlani, T. R.; Gwaltney, S. R.; Hsu, C.-P.; Jung, Y.; Kong, J.; Lambrecht, D. S.; Liang, W.; Ochsenfeld, C.; Rassolov, V. A.; Slipchenko, L. V.; Subotnik, J. E.; Van Voorhis, T.; Herbert, J. M.; Krylov, A. I.; Gill, P. M. W.; Head-Gordon, M. Advances in Molecular Quantum Chemistry Contained in the Q-Chem 4 Program Package. *Mol. Phys.* **2015**, *113* (2), 184–215.

(28) Reiher, M.; Salomon, O.; Artur Hess, B. Reparameterization of Hybrid Functionals Based on Energy Differences of States of Different Multiplicity. *Theor. Chem. Accounts Theory, Comput. Model. (Theoretica Chim. Acta)* **2001**, *107* (1), 48–55.

(29) Becke, A. D. Density-functional Thermochemistry. III. The Role of Exact Exchange. *J. Chem. Phys.* **1993**, *98* (7), 5648–5652.

(30) Lee, C.; Yang, W.; Parr, R. G. Development of the Colle-Salvetti Correlation-Energy Formula into a Functional of the Electron Density. *Phys. Rev. B* **1988**, *37* (2), 785–789.

(31) Weigend, F.; Ahlrichs, R. Balanced Basis Sets of Split Valence, Triple Zeta Valence and Quadruple Zeta Valence Quality for H to Rn: Design and Assessment of Accuracy. *Phys. Chem. Chem. Phys.* **2005**, *7* (18), 3297.

(32) Weigend, F. Accurate Coulomb-Fitting Basis Sets for H to Rn. *Phys. Chem. Chem. Phys.* **2006**, *8* (9), 1057.

(33) Neese, F. The ORCA Program System. *Wiley Interdiscip. Rev. Comput. Mol. Sci.* **2012**, *2* (1), 73–78.

(34) Neese, F. Software Update: The ORCA Program System, Version 4.0. *WIREs Comput. Mol. Sci.* **2018**, *8* (1).

(35) Neese, F.; Wennmohs, F.; Becker, U.; Riplinger, C. The ORCA Quantum Chemistry Program Package. *J. Chem. Phys.* **2020**, *152* (22), 224108.

(36) Pierloot, K.; Vancoillie, S. Relative Energy of the High-(T2g5) and Low-(A1g1) Spin States of [Fe(H2O)6]2+, [Fe(NH3)6]2+, and [Fe(Bpy)3]2+: CASPT2 versus Density Functional Theory. *J. Chem. Phys.* **2006**, *125* (12), 124303.

(37) Stavitski, E.; de Groot, F. M. F. The CTM4XAS Program for EELS and XAS Spectral Shape Analysis of Transition Metal L Edges. *Micron* **2010**, *41* (7), 687–694.

(38) Vankó, G.; Bordage, A.; Pápai, M.; Haldrup, K.; Glatzel, P.; March, A. M.; Doumy, G.; Britz, A.; Galler, A.; Assefa, T.; Cabaret, D.; Juhin, A.; van Driel, T. B.; Kjær, K. S.; Dohn, A.; Møller, K. B.; Lemke, H. T.; Gallo, E.; Rovezzi, M.; Németh, Z.; Rozsályi, E.; Rozgonyi, T.; Uhlig, J.; Sundström, V.; Nielsen, M. M.; Young, L.; Southworth, S. H.; Bressler, C.; Gawelda, W. Detailed Characterization of a Nanosecond-Lived Excited State: X-Ray and Theoretical Investigation of the Quintet State in Photoexcited [Fe(Terpy) 2] 2+. *J. Phys. Chem. C* **2015**, *119* (11), 5888–5902.

(39) Pápai, M.; Vankó, G.; de Graaf, C.; Rozgonyi, T. Theoretical Investigation of the Electronic Structure of Fe(II) Complexes at Spin-State Transitions. *J. Chem. Theory Comput.* **2013**, *9* (1), 509–519.

(40) Rafiq, S.; Fu, B.; Kudisch, B.; Scholes, G. D. Interplay of Vibrational Wavepackets during an Ultrafast Electron Transfer Reaction. *Nat. Chem.* **2021**, *13* (1), 70–76.

(41) Miller, J. N.; McCusker, J. K. Outer-Sphere Effects on Ligand-Field Excited-State Dynamics: Solvent Dependence of High-Spin to Low-Spin Conversion in [Fe(Bpy) 3] 2+. *Chem. Sci.* **2020**, *11* (20), 5191–5204.

(42) Hauser, A. Intersystem Crossing in Fe(II) Coordination Compounds. *Coord. Chem. Rev.* **1991**, *111*, 275–290.

(43) Sárosiné Szemes, D.; Keszthelyi, T.; Papp, M.; Varga, L.; Vankó, G. Quantum-Chemistry-Aided Ligand Engineering for Potential Molecular Switches: Changing Barriers to Tune Excited State Lifetimes. *Chem. Commun.* **2020**, *56* (79), 11831–11834.

(44) Kunnus, K.; Vacher, M.; Harlang, T. C. B.; Kjær, K. S.; Haldrup, K.; Biasin, E.; van Driel, T. B.; Pápai, M.; Chabera, P.; Liu, Y.; Tatsuno, H.; Timm, C.; Källman, E.; Delcey, M.; Hartsock, R. W.; Reinhard, M. E.; Koroidov, S.; Laursen, M. G.; Hansen, F. B.;

Vester, P.; Christensen, M.; Sandberg, L.; Németh, Z.; Szemes, D. S.; Bajnóczi, É.; Alonso-Mori, R.; Glownia, J. M.; Nelson, S.; Sikorski, M.; Sokaras, D.; Lemke, H. T.; Canton, S. E.; Møller, K. B.; Nielsen, M. M.; Vankó, G.; Wärnmark, K.; Sundström, V.; Persson, P.; Lundberg, M.; Uhlig, J.; Gaffney, K. J. Vibrational Wavepacket Dynamics in Fe Carbene Photosensitizer Determined with Femtosecond X-Ray Emission and Scattering. *Nat. Commun.* **2020**, *11* (1), 1–11.

(45) Hainer, F.; Alagna, N.; Reddy Marri, A.; Penfold, T. J.; Gros, P. C.; Haacke, S.; Buckup, T. Vibrational Coherence Spectroscopy Identifies Ultrafast Branching in an Iron(II) Sensitizer. *J. Phys. Chem. Lett.* **2021**, *12* (35), 8560–8565.

(46) Scheidt, W. R.; Durbin, S. M.; Sage, J. T. Nuclear Resonance Vibrational Spectroscopy--NRVS. *J. Inorg. Biochem.* **2005**, *99* (1), 60–71.